PAPER

Efficient computation of the angularly resolved chord length distributions and lineal path functions in large microstructure datasets

Efficient computation of the angularly resolved chord length distributions and lineal path functions in large microstructure datasets

David M. Turner[1], Stephen R. Niezgoda[2,3], and Surya R. Kalidindi[1,a]

[1]George W. Woodruff School of Mechanical Engineering, Georgia Institute of Technology, Atlanta GA 30332
[2]Department of Materials Science and Engineering, The Ohio State University, Columbus OH 43210
[3]Department of Mechanical and Aerospace Engineering, The Ohio State University, Columbus OH 43210
[a]Author to whom correspondence should be addressed

Abstract

Chord length distributions (CLDs) and lineal path functions (LPFs) have been successfully utilized in prior literature as measures of the size and shape distributions of the important microscale constituents in the material system. Typically, these functions are parameterized only by line lengths, and thus calculated and derived independent of the angular orientation of the chord or line segment. We describe in this paper computationally efficient methods for estimating chord length distributions and lineal path functions for 2-D (two dimensional) and 3-D microstructure images defined on any number of arbitrary chord orientations. These so called fully angularly resolved distributions can be computed for over 1000 orientations on large microstructure images (500^3 voxels) in minutes on modest hardware. We present these methods as new tools for characterizing microstructures in a statistically meaningful way.

Keywords: *chord length distribution, lineal path function, image analysis*

1. Introduction

In recent years, the field of materials science and engineering has significantly advanced our understanding of how materials processing parameters influence the complex, hierarchical, internal structure (hereafter simply referred to as the microstructure) of advanced engineering materials, which in turn dominates the macroscale properties and performance exhibited by the material. This improved understanding has led to impressive advances in the development of highly sophisticated, physics-based or microstructure-sensitive, material models which are being integrated into commercial design and simulation software. Concurrently, major advances in 3-D (three dimensional) and 4-D (3-D and time resolved) materials characterization have set the stage for the affordable and accelerated deployment of new/improved materials for engineering technologies through the continued adoption of Integrated Computational Materials Engineering (ICME)[1–8], as envisioned by the materials genome initiative (MGI).

The ICME strategy of replacing combinatoric experimentation with simulation, is dependent on verification and validation of not only the mathematical models used in the simulation but also of the simulation inputs as well. One of the key challenges of computational design is the validation of mesoscale materials/microstructure simulation volume elements, either representative volumes [1-12] or statistical volume elements [11, 12] as inputs to property models or digitally generated microstructures resulting from thermo-mechanical processing. Many advanced microstructural metrics have been proposed in literature to describe the shape and spatial distribution of microstructural features, including the *n*-point spatial correlations [13-20], shape moment invariants [21], topological descriptors including homology [22-24], entropic descriptors [25, 26], etc. However, for many applications, the cost of calculating and interpreting these descriptors is not appropriate. Instead, simple stereological estimators such as intercept lengths are mostly employed due to their a) easy interpretation, b) straightforward manual calculation using widely available microscopy software tools such as ImageJ [27], and c) strong connection to properties relevant to design (for example, grain shape and size distributions in polycrystalline metals are known to strongly influence their mechanical strength [28-32], while pore size

and shape distributions are known to have a dominant effect on the mechanical and transport properties in porous solids [13, 33]). Typically, only mean or average feature sizes are calculated by application of the broadly adopted ASTM E-112 "Standard Test Methods for Determining Average Grain Size" protocols [34], which involve counting intercepts of randomly oriented lines on two-dimensional sections or counting numbers of grains per area. The obvious weakness of such approaches is that they are not applicable to structures that have large structural anisotropies or where the size distribution of features includes distinct populations of several large and small features. The limited number of features counted also means that rare features corresponding to the extreme tails of the size distributions are unlikely to be counted. The manual or semi-automated nature of the analysis can also be problematic in that great care must be taken to ensure that the results are independent of who is performing the analysis, as large variances can result. For example, ASTM E-112 gives reproducibility at ± 0.5 G which corresponds to $\approx \pm 9\mu m$ uncertainty in the average diameter for material with $45\mu m$ average grain diameter.

In this work, we demonstrate a computationally efficient scheme to compute anisotropic microstructure chord length distributions, which capture the complete size distribution of microstructure features in two- or three-dimensional material datasets. This approach retains the main benefits of the average intercept techniques in that the results are quick to compute, and simple to interpret and visualize, while providing significantly more detailed information beyond the average feature size.

Chord length distributions (CLDs) [35-43] have been successfully utilized in prior literature as rigorous measures of the size and shape distributions of the important microscale constituents in the material system. A chord is defined as any line segment in the microstructure whose interior points are all occupied by the specific local state of interest (e.g., a pore or a distinct phase) and the end points abut against other local states. In other words, chords cannot be extended in either direction and still remain completely in the local state region of interest. Formally, the CLD, $p^i(\mathbf{z})$, denotes the probability density associated with finding a chord $\mathbf{z}$ (including a specified magnitude and a specified direction) within the

local state i in a given microstructure dataset. When the chords are identified by both their length and direction, the resulting distributions are termed as angularly resolved CLDs in this work.

Another important microstructure metric that is closely related to the chord length distribution is the lineal path function (LPF) [13, 44]. Formally, the LPF, $L^i(\mathbf{z})$, denotes the probability that a line segment $\mathbf{z}$ (including a specified magnitude and a specified direction) thrown randomly into a given microstructure dataset lies entirely within local state i. In this definition, the line segment does not have to be a chord with end points at the interfaces as defined earlier. As before, when the line segments are identified by both their length and direction, the resulting function is termed as the angularly resolved LPF in this work.

Prior work [37] has established a relationship between the CLD and the LPF. This relationship can be expressed as

$$p^i(\mathbf{z}) = \frac{l_c}{V^i}\frac{d^2L^i(\mathbf{z})}{dz^2}, \qquad l_c = \int_0^\infty z p^i(\mathbf{z}) dz \tag{1}$$

where z is the magnitude of $\mathbf{z}$, V^i is the volume fraction of local state i, and l_c is the mean chord length along the direction of $\mathbf{z}$. Both the CLD and the LPF are commonly estimated by sampling, and accurate estimation requires identifying a very large number of chords in the microstructure or throwing a very large number of line segments into the microstructure. Because of the high computational cost involved in these estimations, most prior applications [13, 35-43, 45, 46] have been largely limited to isotropic structures, where the CLD and the LPF were assumed to be independent of the direction of the chord or the line segment, respectively.

It should also be noted that CLDs and LPFs have been utilized successfully in reconstructions of microstructures [47]. More germane to the present discussion, Talukdar et al. [48] utilize angularly resolved CLDs in their microstructure reconstructions. However, they employ only four selected directions in a two-dimensional (2-D) microstructure dataset in computing the angularly resolved CLDs.

This is presumably because of the prohibitively high computational cost involved in the currently used methods for estimating these distributions. In fact, Talukdar et al. [48] utilize a sampling approach for the calculation of the CLDs by translating a line successively to every pixel in the image. This approach has the unique advantage that it does sample all chords present in the given dataset. Singh et al. [44] use a similar approach for computing the lineal path function for high resolution 2D micrographs. They compute angularly resolved lineal path functions in three directions; zero degrees, ninety degrees, and forty-five degrees. However, certain optimizations are needed to make the approach computationally practical for use in large 2-D and 3-D microstructure datasets, while including a larger number of directions.

The main purpose of this paper is to explore an efficient algorithm for computation of angularly resolved CLDs and LPFs. The approach shown in this paper is referred as the Scan Line Method, and is an extension of the simple idea of translating a line successively to every pixel in the dataset (utilized earlier by Talukdar et al. [48] and Singh et al. [44]). We present in this paper several new ideas for optimization of the computations involved in the Scan Line Method for estimating angularly resolved CLDs in large 2-D and 3-D microstructure datasets. Furthermore, we present numerical procedures for extracting LPFs from the computed CLDs in this approach. The protocols developed in this work are demonstrated on selected example 2-D and 3-D microstructure datasets. We show clearly that angularly resolved CLDs and LPFs can be computed efficiently for large 3D microstructures for large numbers of directions.

2. Computational Procedures

A line scan approach, such as the one employed by Talukdar et al. [48], might prove to be computationally efficient if implemented in a highly optimized environment. As an illustrative example, consider a 2-D binary image represented as a square matrix I. Furthermore, let us restrict our initial attention to only the chords in this image that have an orientation of 0°, i.e., those that are completely horizontal. We can precisely identify and compute the distribution of lengths of these chords by simply scanning through the rows of the matrix I (assuming these correspond to pixels in the horizontal

direction), and keeping track of the starts and ends of chords as we encounter them. For instance, we can scan along each pixel in a row of the image and record when we encounter a phase value of interest. After this, we will continue scanning forward until we encounter a pixel with a value of another phase. At this point, we will have identified a chord of a certain length and it can be recorded for calculation of a distribution. This approach works just as well for vertical chords as we can simply look at the columns of the image. One final note is that we must discard chords that originate or touch the boundary of the image because we cannot be sure these are in fact chords. This is because pixel\voxels at the edge of our image may not be interface pixels\voxels. The criteria of non-edge chords not being counted can be removed when one wishes to calculate lineal path functions from chord length distributions because lineal path functions do not require that line segments span interfaces like chords.

A scanning algorithm for orthogonal lines is extremely efficient both computationally and in terms of memory. It will require on the order of $O(n)$ number of operations, where n is the number of pixels in the image. The memory requirements are even better as it requires only keeping track of a distribution of chord lengths, where the zero chord length and the longest possible chord lengths define the range. So we have a memory requirement upper bound of $O(n)$ because the computation can be done in place. However, we must be able to adapt this algorithm for chords that are not perfectly aligned along the reference axes of our image. Fortunately, the field of computer graphics has already developed a fast and simple algorithm for determining arbitrarily oriented scan lines through an image. This novel idea is described below.

Bresenham's line drawing algorithm [49] is efficient algorithm for drawing an approximation of a line between two points in an n-dimensional image. Given the start and endpoint of the line in the image, Bresenham's algorithm determines the pixels lying on the line between these two points using only integer addition, subtraction, and bit shifting. Using only integer arithmetic is not only faster, but more accurate because it avoids the common drawbacks of accumulated floating point error. With Bresenham's algorithm, we can determine the pixels that correspond to a scan line through the image of any

orientation. Once we have determined the pixels for a given scan line, we can then simply translate this line such that it sweeps through the entire image (see Figure 1).

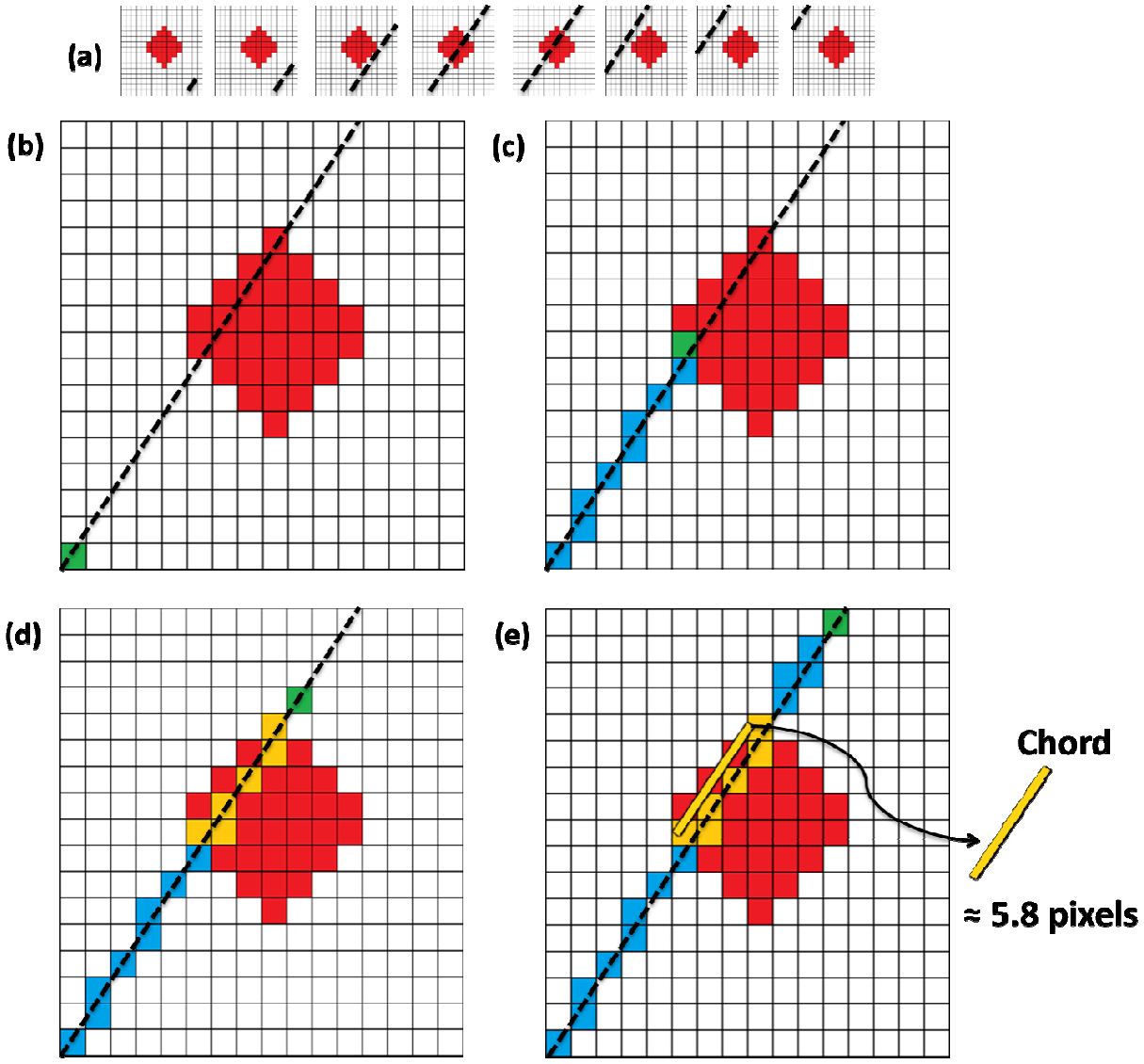

Figure 1: This figure details how chords are identified for a particular orientation. In all images the red phase is the phase of interest. The green coloured pixel marks the active pixel in the algorithm, blue marks pixels that have be processed, and gold marks pixels along a chord. In (a) we show how for a given orientation we try every scanline within the image dimensions. Some are not shown here for the sake of brevity. For each scanline, we begin (b) by starting at one edge of the image and marching along the rasterized approximation of an oriented line until (c) we encounter the phase of interest. We then continue moving along the scanline until (d) we encounter a pixel that is not the phase of interest. At this point we have identified a chord as long as the start pixel and end pixel are not touching the edge of the image. In (e) we continue processing the remaining portion of the scanline.

Angularly resolved chord length distributions and lineal path functions

Using translated Bresenham lines we can scan through an image in any arbitrary direction and identify all chords in the local state regions of interest. This scan converted image will allow us to calculate the distribution of chord lengths in that direction using a process that is almost identical to the case of vertical or horizontal chords described earlier. The main difference is that we will have to account for the conversion between number of pixels along a Bresenham line and the length of the line. The length of a chord can be approximated by calculating the Euclidean distance between the chords start and end pixels.

This scan line approach is roughly equivalent to the rotation of a discretized image. Computationally, the rotation of an image is worse than the scan line method described above since it requires a copy of the image to be made. However, because 2D image rotation is such a common image operation in computer graphics, a tremendous amount of work has been done to develop optimized routines for this purpose. We have thus implemented two algorithms for 2D images, one uses the above described scanline approach and the other using simple image rotation with bilinear interpolation. Bilinear interpolation is probably the most common interpolation method used for image registration to a new coordinate system. Given a point to register, it finds the four nearest pixels and computes weighted average of their values [50]. Our results in this paper for 2-D images are shown and compared for both methods. However, such a simple approach of rotating the image was not effective for 3D images for two principal reasons. First, there are no real efficient implementations of 3D image rotation algorithms known to the authors. Memory requirements of copying a large 3D image could be prohibitive; therefore, an in-place algorithm like the scan line method is more attractive in the authors' opinion.

The same scanline algorithm outlined above for 2-D images can be extended to 3-D images as well. We have developed a parallelized implementation of this algorithm that computes a full angularly resolved CLD. Performance of this algorithm running on an 8 core 2.4 GHz Intel Xeon machine for a 500^3 voxel dataset with azimuthal and polar angular resolution of 5^o was approximately 20 minutes. This algorithm may be significantly improved if it was developed for modern graphics processing units

(GPUs) because of its massively parallel nature. That is, each computation for a specific scan line orientation is completely independent of the others.

It is relative easy to compute the lineal path function directly from a chord length distribution. Such an algorithm is described by Singh et al. [44] and simply requires counting all the line segments that could possibly fall along each chord. That is, if we have a chord of length 10 pixels\voxels. Then we can fit one line of length 10, two of length 9, three of length 8, and so on. The only thing left after enumerating all such line segments is to normalize by the total number of possible line segments for each length which is a function of the image dimensions and line length. One important note, as mentioned before, is that chords that touch the boundary of the image should be added when constructing lineal path functions from chord length distributions.

3. Results

To demonstrate our algorithms we have selected a set of example microstructures (both 2-D and 3-D samples).

3.1 Two-Phase 2-D Microstructure

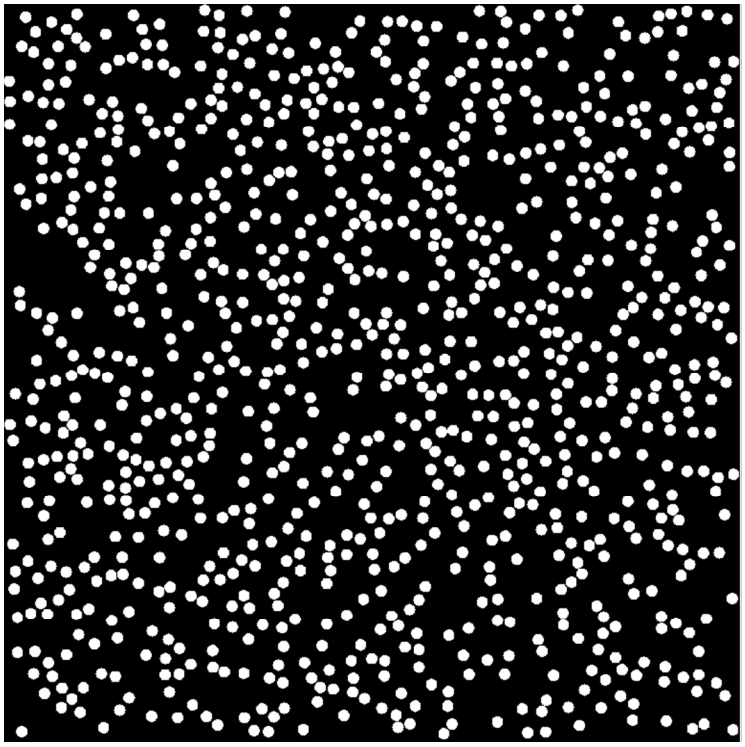

Figure 2: A simple image of identical circles of diameter of approximately 32 pixels placed in a uniformly random manner. Volume fraction of the circular phase is 18.2%. The image dimensions are 2048x2048.

As a first demonstration, we consider a simple 2-D digital microstructure (shown in Figure 2) with a uniformly random distribution of circles each with a diameter of approximately 32 pixels. Volume fraction of the circular phase is 18.2 percent. The diameter is approximate because of the nature of representing a circle on a raster. The main advantage of selecting such a simple example microstructure is that we have a closed form analytical solution for both the CLD and LPF. For many simple convex shapes/bodies, closed form expressions for the non-angularly resolved CLD have been derived and studied [37, 51-53]. For a simple circle, we have the following expression [51] for the non-angularly resolved CLD:

$$p(z) = \frac{z}{4R\sqrt{R^2 - \left(\frac{z}{2}\right)^2}} \tag{2}$$

where R is the radius of the circle, which is 16 pixels for our test image described above. A comparison of the integrated values recovered using our algorithm (rotated 2D images) with the closed form expression (**2**) is presented in Figure 3. We can see that the calculation is accurate aside from the noise present due to the discretized nature of the rasterized circle. That is, our digitized image of a circle is only an approximation to a true circle made from a discrete set of Bresenham lines. Therefore, certain chords are overrepresented and others are underrepresented. Nowhere is this more obvious than in the regime of very short chords (around 1 to 3 pixels). Several authors [42, 51] discuss this problem and its causes extensively, and describe a few very simple mitigation strategies. These simple strategies generally involve discarding certain chords by defining a minimum acceptable chord length criterion. The strictest of these criteria is that in order for a chord to be counted it must at least traverse a distance of one voxel unit size in all dimensions. That is, we only accept chords that traverse at least a single resolution distance in both x and y for 2D and x, y, and z for 3D. We have not implemented this criterion in the calculations shown in Figure 3, so that we can illustrate the inherent inaccuracies of approximating chords and shapes on a raster. In Figure 4, we show a comparison between results computed using the scanline method and the image rotation methods described above which show general agreement. We would like to note that the rotation method seemed to result in a slightly less noisy result when compared to the scan line approach. We conjecture that this is a result of the bilinear interpolation and thresholding of the image when it is rotated. Our hypothesis would be that scan line method captures the discretized nature of the circle at different angles more accurately, while the image rotation method has a tendency to average out these differences at each orientation. Further work is needed to verify this hypothesis.

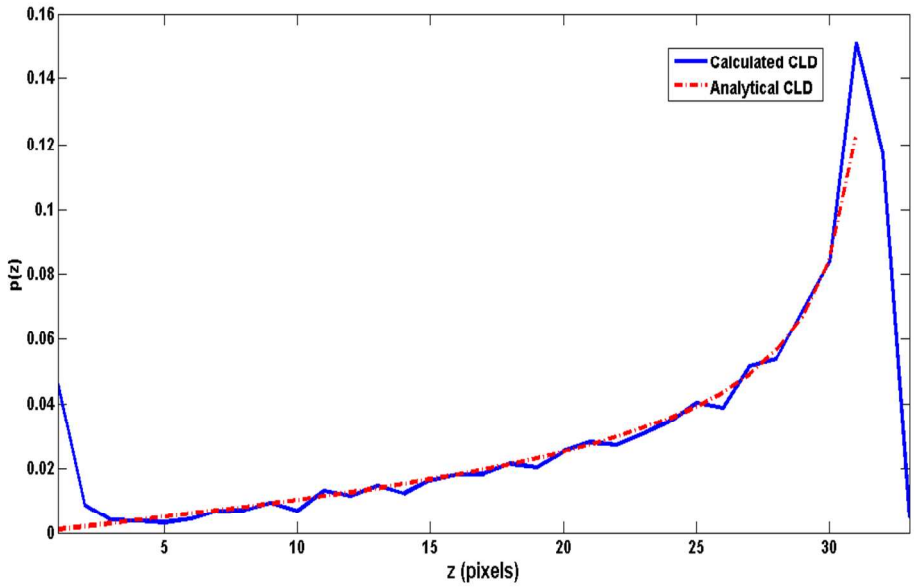

Figure 3: Comparison of closed form and calculated results for non-angularly resolved chord length distribution for a simple two dimensional circle with an approximate diameter of 32 pixels.

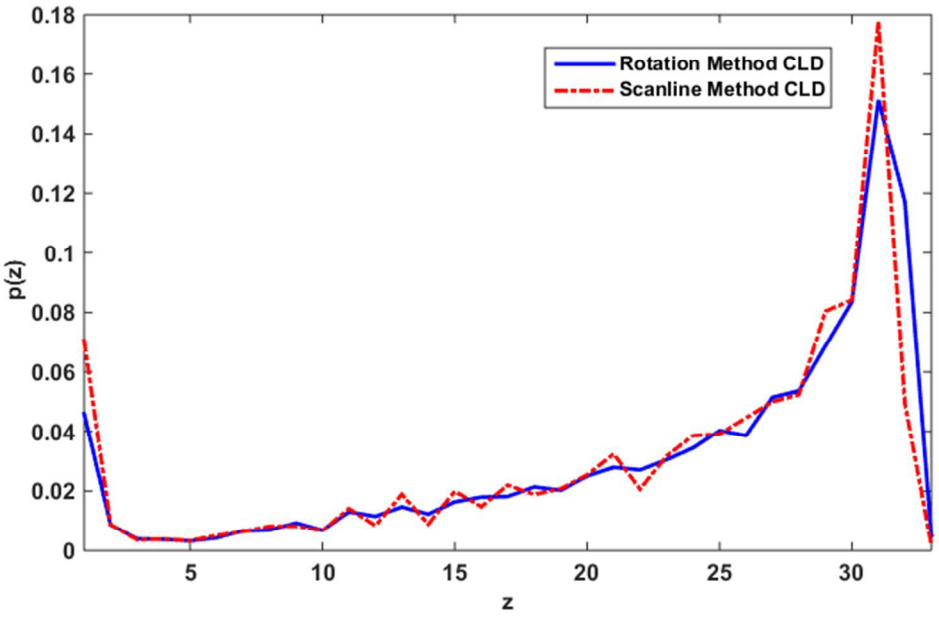

Figure 4: Comparison between chord length distributions computed using both a scanline and image rotation method. Aside from some small deviations due to the differences between Bresenham line discretization and image rotation interpolation, the methods mostly agree.

Angularly resolved chord length distributions and lineal path functions

If we do not integrate over the angular dependence of the chord length distribution, we arrive at the results shown in Figure 5. This figure depicts the chord length distribution for each angle sampled, where each exhibits inherent noise as shown in Figure 3. However, based on how the circle is rasterized, certain chord orientations will exhibit more noise than others. To alleviate this noise, we have performed a five point/pixel moving window average on each distribution (for each sampled angle). These results show, as we expect, that there is no angular dependence on the chord length distribution for a circle. The computation of the angularly resolved full distribution for a 500x500 pixel image took less than a second on a 2.00 GHz Pentium 4 PC.

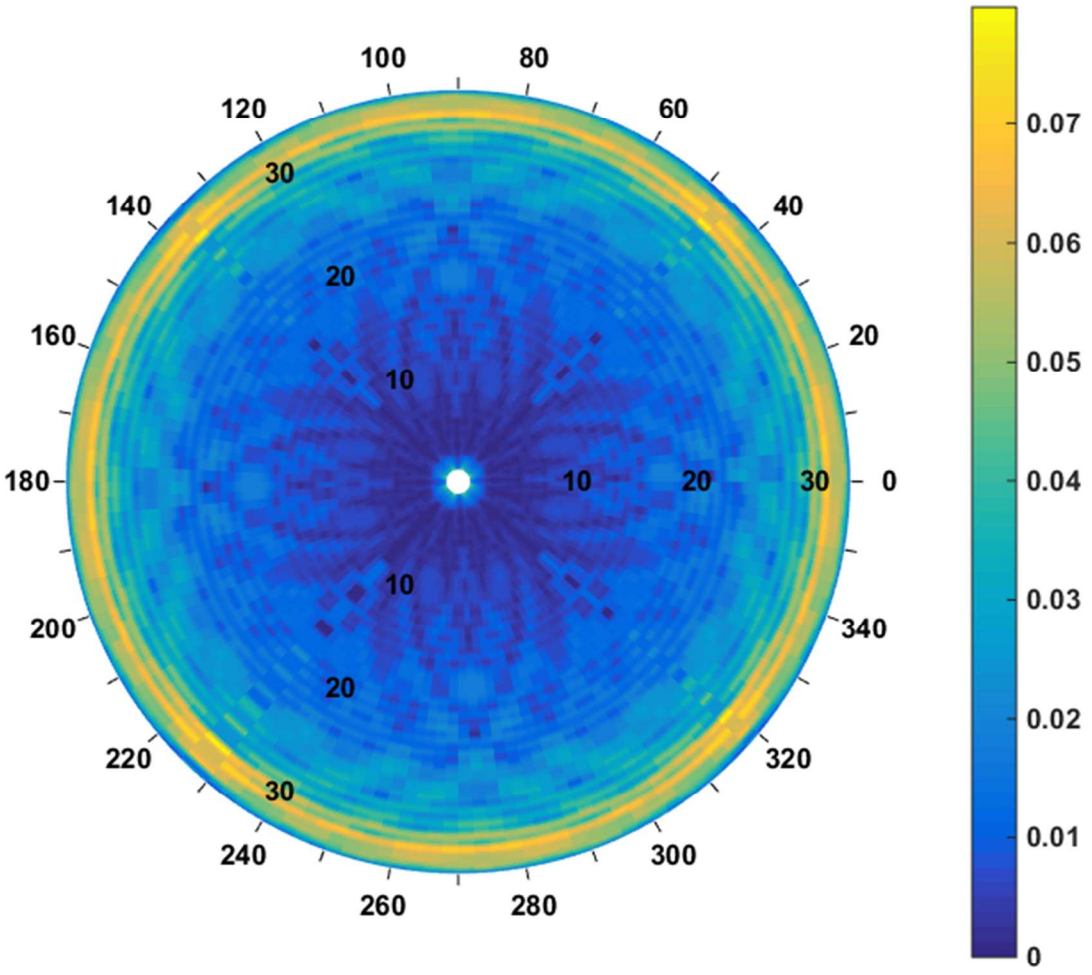

Figure 5: Full angularly resolved chord length distribution for the image in Figure 2. The polar axis on the figure represents the angular orientation of the chord. The radial axis represents the length of the chord. Each individual distribution (chord angle) has been smoothed with a 5 point/pixel moving window average to eliminate noise resulting from discretization of the circle.

To confirm our calculation of LPFs from our chord length distribution, similar to [44], we used the following expression for the LPF of the matrix phase for a set of uniformly distributed equal size circles;

$$L^{matrix}(\mathrm{z}) = V^{matrix} e^{-\frac{2\left(1-V^{matrix}\right)z}{R\pi V^{matrix}}} \tag{3}$$

The V^{matrix} is the volume fraction of the matrix phase, 81.8 percent in our case. The radius R of our circles is 16 pixels as described in Figure 2. The comparison of the calculated and analytical LPF is shown in Figure 6. The results show excellent agreement between the two functions.

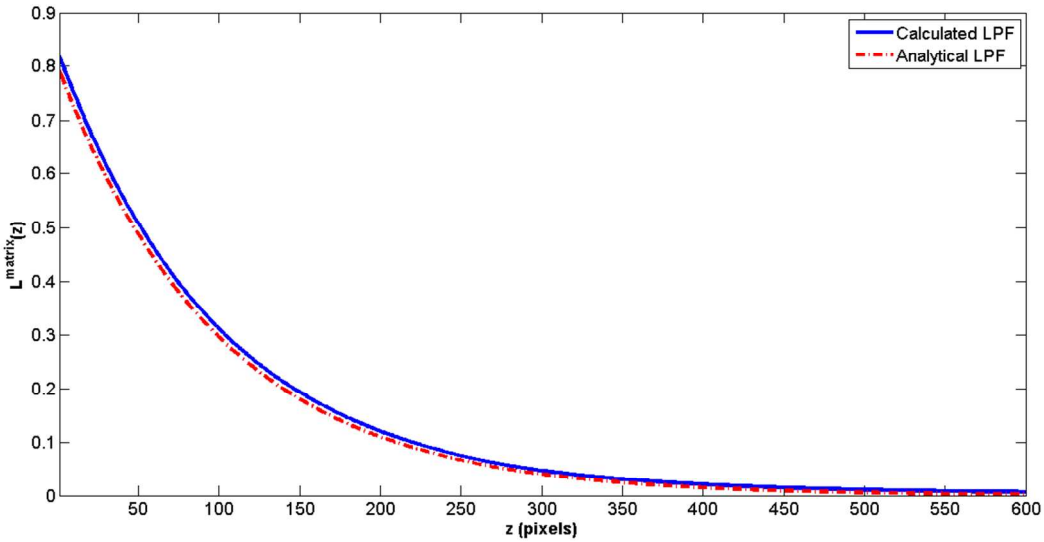

Figure 6: Shows a comparison between the analytical and calculated LPFs for the matrix phase in the case of randomly distributed circles of r 32 pixels. The calculated LPF derived from our chord length distribution of the matrix phase of the image presented in Figure 2 show excellent agreement.

To demonstrate the capability of the angularly resolved chord length distributions in capturing the anisotropic details of the microstructure, we have selected another simple synthetic 2D microstructure as a case study. In this example, the image comprised of uniform randomly placed ellipses with major axis of 95 pixels and minor axis of 63 pixels. The ellipses are all oriented with the major axis being vertical. This microstructure is shown in Figure 7, and its corresponding angularly resolved chord length distribution is shown in Figure 8. As seen from these figures, the proposed protocols do provide the expected results. This specific example, however, does not have a closed-form analytical solution (the solutions available in literature [54] are for the case where the chords are not angularly resolved).

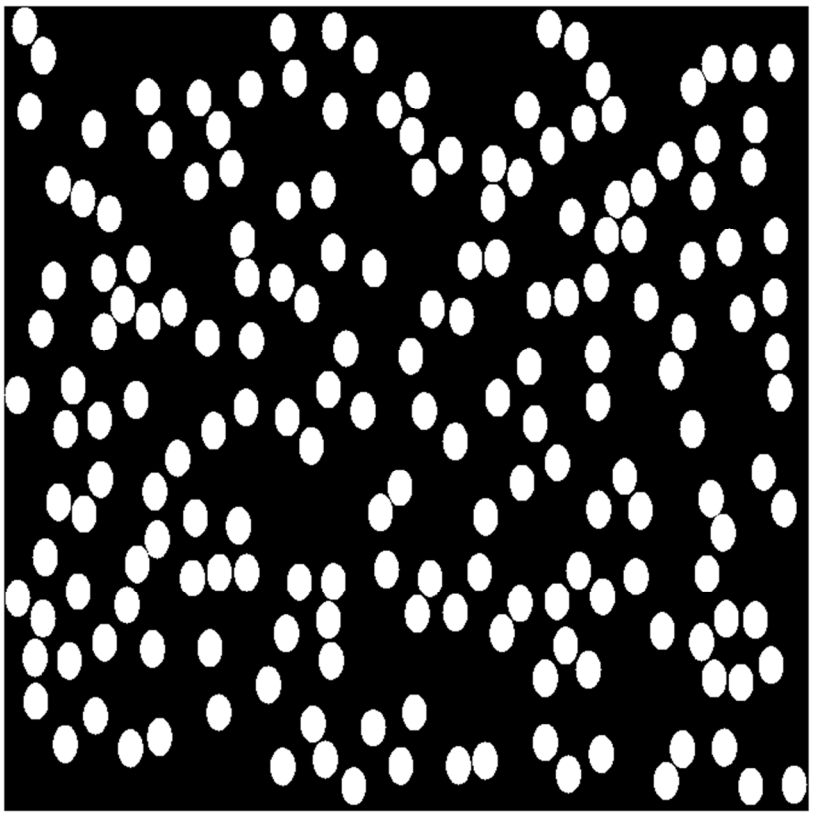

Figure 7: image of uniform randomly placed ellipses with major axis of 95 pixels and minor axis of 63 pixels. The ellipses are all oriented with major axis at 90 degrees from the horizontal.

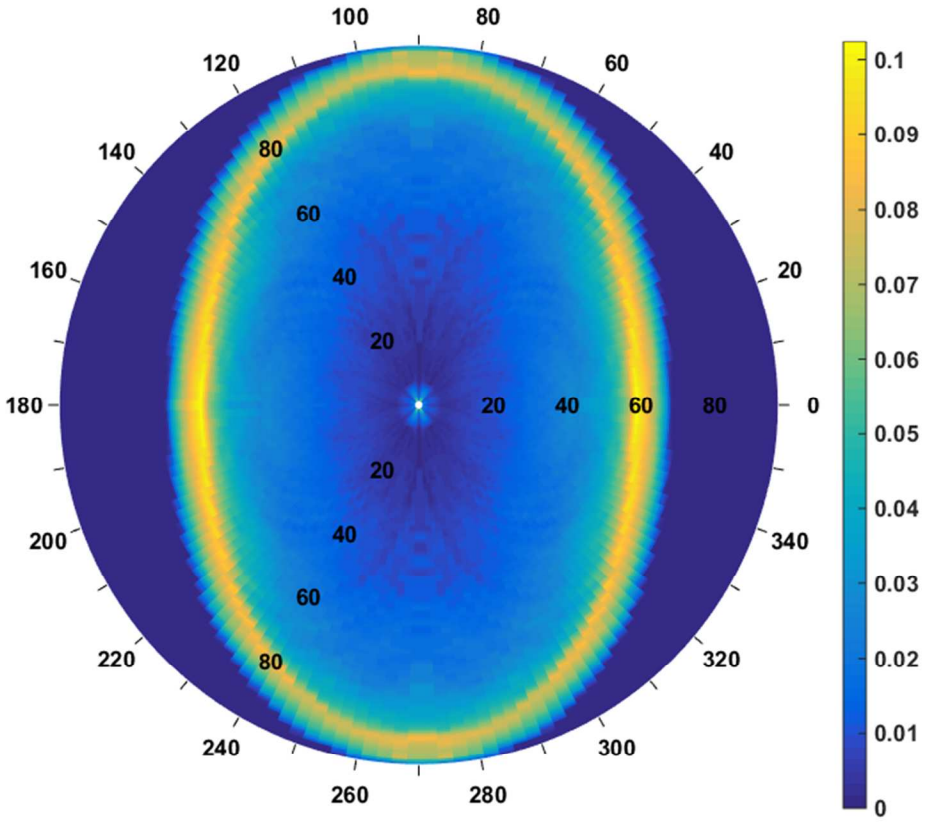

Figure 8: The angularly resolved chord length distribution of the image shown in figure 7. The 95 pixel major axis of the ellipse is highlighted by the peak of the chord length distribution at the 90 degree orientation.

3.2 Porous 3-D Microstructure

To illustrate the capabilities of the extended approach described in this paper for 3-D microstructures, we have selected a digitally simulated 3D porous microstructure. This high resolution sample consists of 500x500x500 cubic voxels. It has been segmented into two distinct phases: pore and matrix. To quantify the shape of the porous structure, we ran our chord length algorithm on the pore phase of this dataset. We used scanlines at azimuthal and polar angular increments of every 5 degrees.

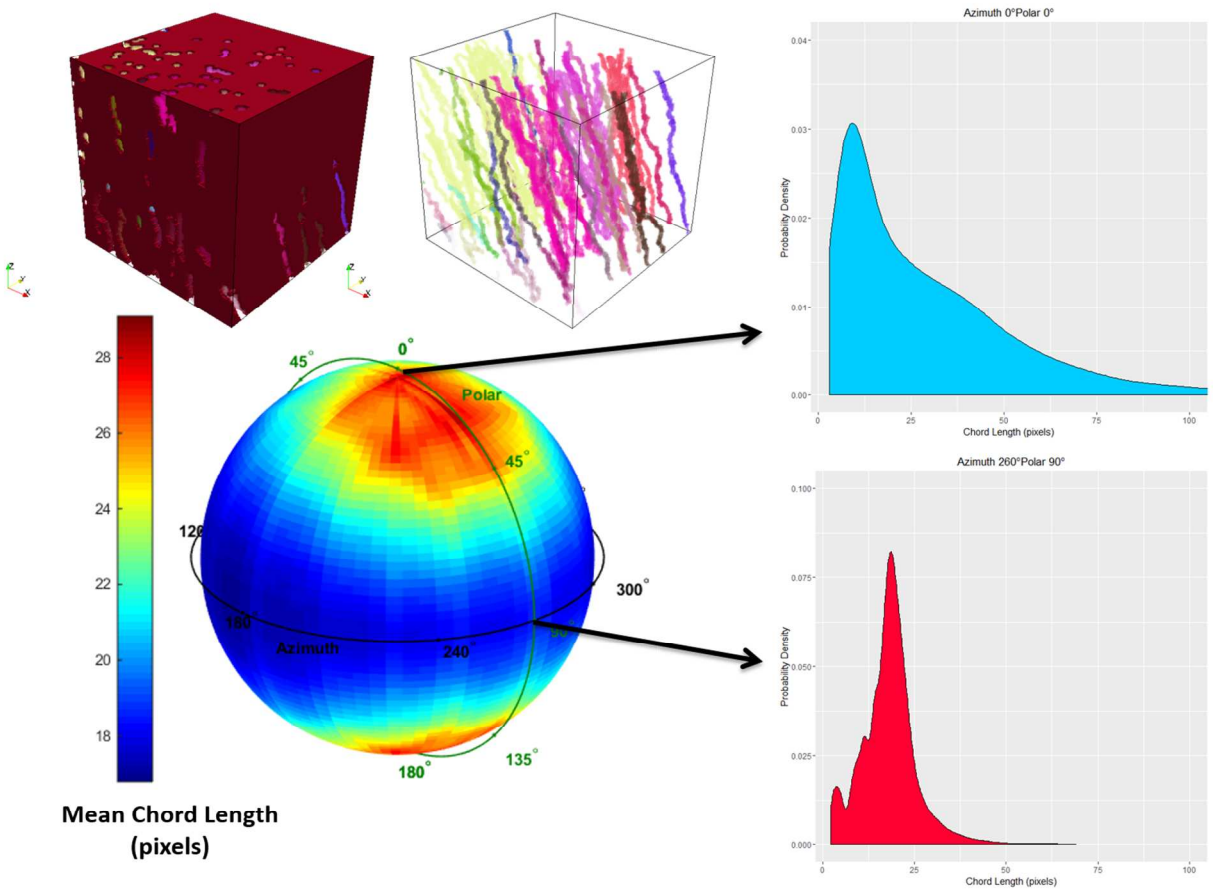

Figure 9: Top left shows a synthetic digitally created 3-D microstructure. The pore network has been colored to show connected pores with distinguishing colors. In the bottom left, the mean pore chord length in all directions has been plotted on the surface of a sphere. Polar and azimuthal angles correspond to orientations of the chord within the sample. To the right, we show selected chord length distributions for two chord orientations. The angularly resolved chord length distributions show clearly the anisotropic nature of the porous structure.

Analysis of these results shows a difference of approximately 11 voxels between the maximum and minimum mean chord lengths for sampled directions. These anisotropic features of the pores in this sample are illustrated in Figure 9. It is important to remember that for each chosen orientation of scanlines through the sample we calculate a full chord length distribution. It is difficult to render all of this information into a single figure so we have elected to show an illustrative subset of these distributions. Typical calculations of a non-angularly resolved chord length distribution would obviously not capture these features. Calculation of these distributions on the entire 500x500x500 voxel dataset was performed using a dual core Intel® i7-2460M CPU at 2.8 GHz in roughly 20 minutes.

4. Summary

Despite the known complex anisotropic nature of materials, non-angularly resolved implementations of the chord length distribution and lineal path function are frequent in the literature. We have described an efficient algorithm for the calculation of the angularly resolved chord length distributions in both 2D and 3D digital images. To the author's knowledge, this work presents the first calculations of these angularly resolved distributions for high resolution 3D datasets in thousands of directions at once. Moreover, we believe the algorithm presented can be extended to leverage general purpose computing on graphics processing units (GPGPU) to reach an additional order of magnitude or more performance increase. These results should provide researchers wishing to quantify the structure of materials with a new and more efficient tool to do so.

Acknowledgements

DT and SK acknowledge funding from the Office of Naval Research (ONR) award N00014-15-1-2478 (Dr. William M. Mullins, program manager).

References

1. Hill, R., *Elastic properties of reinforced solids: some theoretical principles.* Journal of the Mechanics and Physics of Solids, 1963. **11**: p. 357-372.
2. Beran, M.J., *Statistical continuum theories*. 1968, New York: Interscience Publishers.
3. Hazanov, S. and C. Huet, *Order relationships for boundary conditions effect in heterogeneous bodies smaller than the representative volume.* Journal of the Mechanics and Physics of Solids, 1994. **42**(12): p. 1995-2011.
4. Drugan, W.J. and J.R. Willis, *A micromechanics-based nonlocal constitutive equation and estimates of representative volume element size for elastic composites.* Journal of the Mechanics and Physics of Solids, 1996. **44**(4): p. 497-524.
5. Huet, C., *Application of variational concepts to size effects in elastic heterogeneous bodies.* Journal of the Mechanics and Physics of Solids, 1990. **38**(6): p. 813-841.
6. Kanit, T., et al., *Determination of the size of the representative volume element for random composites: statistical and numerical approach.* International Journal of Solids and Structures, 2003. **40**(13-14): p. 3647-3679.
7. Sab, K., European Journal of Mechanics A/Solids. **11**: p. 505.
8. Willis, J.R., *Variational and related methods for the overall porperties of composite materials.* Advances in Applied Mechanics, 1981. **21**: p. 2-78.
9. Ostoja-Starzewski, M., *Microstructural randomness and scaling in mechanics of materials*. 2007: CRC Press.

10. Kröner, E., *Berechnung der elastischen Konstanten des Vielkristalls aus den Konstanten des Einkristalls.* Zeitschrift für Physik, 1958. **151**(4): p. 504-518.
11. Niezgoda, S.R., et al., *Optimized structure based representative volume element sets reflecting the ensemble-averaged 2-point statistics.* Acta Materialia, 2010. **58**(13): p. 4432-4445.
12. Qidwai, S.M., et al., *Estimating response of polycrystalline materials using sets of weighted statistical volume elements (WSVEs).* Acta Materialia, 2012. **60**: p. 5284–5299.
13. Torquato, S., *Random Heterogeneous Materials*. 2002, New York: Springer-Verlag.
14. Adams, B.L., H. Garmestani, and G. Saheli, *Microstructure design of a two phase composite using two-point correlation functions.* Journal of Computer-Aided Materials Design, 2004. **11**: p. 103–115.
15. Tewari, A., et al., *Quantitative characterization of spatial clustering in three-dimensional microstructures using two-point correlation functions.* Acta Materialia, 2004. **52**(2): p. 307-319.
16. Gokhale, A.M., *Experimental measurements and interpretation of microstructural N-point correlation functions.* Microscopy and Microanalysis, 2004. **10**(SUPPL. 2): p. 736-737.
17. Gokhale, A.M., A. Tewari, and H. Garmestani, *Constraints on microstructural two-point correlation functions.* Scripta Materialia, 2005. **53**: p. 989-993.
18. Huang, M., *The n-point orientation correlation function and its application.* International Journal of Solids and Structures, 2005. **42**(5-6): p. 1425-1441.
19. Etingof, P.I., D.D. Sam, and B.L. Adams, *Tensorial representation of two-point correlation functions for polycrystalline microstructure by harmonic polynomials.* Philosophical Magazine A: Physics of Condensed Matter, Defects and Mechanical Properties, 1995. **72**(1): p. 199.
20. Niezgoda, S.R., D.T. Fullwood, and S.R. Kalidindi, *Delineation of the space of 2-point correlations in a composite material system.* Acta Materialia, 2008. **56**(18): p. 5285-5292.
21. MacSleyne, J.P., J.P. Simmons, and M. De Graef, *On the use of 2-D moment invariants for the automated classification of particle shapes.* Acta Materialia, 2008. **56**(3): p. 427-437.
22. Kaczynski, T., K. Mischaikow, and M. Mrozek, *Computational homology*. Vol. 157. 2006: Springer Science & Business Media.
23. Gerrard, D.D., et al., *Computational Homology, Connectedness, and Structure-Property Relations.* Computers, Materials, & Continua, 2010. **15**(2): p. 129-152.
24. Niezgoda, S.R., et al., *Applications of the phase-coded generalized hough transform to feature detection, analysis, and segmentation of digital microstructures.* Computers, Materials, & Continua, 2010. **14**(2): p. 79-98.
25. Piasecki, R. *Microstructure reconstruction using entropic descriptors*. in *Proceedings of the Royal Society of London A: Mathematical, Physical and Engineering Sciences*. 2011. The Royal Society.
26. Balzani, D., et al., *Construction of two- and three-dimensional statistically similar RVEs for coupled micro-macro simulations.* Computational Mechanics, 2014. **54**(5): p. 1269-1284.

27. Abràmoff, M.D., P.J. Magalhães, and S.J. Ram, *Image processing with ImageJ.* Biophotonics international, 2004. **11**(7): p. 36-43.
28. Petch, N.J., *Cleavage strength of polycrystals.* Iron and Steel Institute -- Journal, 1953. **174**(Part 1): p. 25-28.
29. Hall, E.O., *The deformation and ageing of mild steel III. Discussion of results.* Proceedings of the Physical Society. Section B, 1951. **64**: p. 747-753.
30. E. El-Danaf, S.R.K., R.D. Doherty, *Influence of grain size and stacking-fault energy on deformation twinning in FCC metals.* Metallurgical and Materials Transactions A, 1999. **30**: p. 1223-1233.
31. Morrison, D.J. and J.C. Moosbrugger, *Effects of grain size on cyclic plasticity and fatigue crack initiation in nickel.* Int. J. Fatigue, 1997. **20**: p. S51-59.
32. Fromm, B.S., et al., *Grain size and orientation distributions: Application to yielding of alpha-titanium.* Acta Materialia 2009. **57**: p. 2339–2348.
33. Liang, Z., M.A. Ioannidis, and I. Chatzis, *Permeability and electrical conductivity of porous media from3D stochastic replicas of the microstructure.* Chem. Eng. Sci., 2000. **55**(22): p. 5247-5262.
34. E-112, A., *Standard test methods for determining average grain size*, 2010, ASTM International USA.
35. Shah, A.P., et al., *A Comparison of Skeletal Chord-Length Distributions in the Adult Male.* Health Physics, 2005. **89**(3): p. 199-215 10.1097/01.HP.0000164653.55582.fd.
36. Gille, W., D. Enke, and F. Janowski, *Pore Size Distribution and Chord Length Distribution of Porous VYCOR Glass (PVG).* Journal of Porous Materials, 2002. **9**(3): p. 221-230.
37. Torquato, S. and B. Lu, *Chord-length distribution function for two-phase random media.* Physical Review E, 1993. **47**(4): p. 2950.
38. Darley, P.J., *Measurement of linear path length distributions in bone and bone marrow using a scanning technique.* Journal Name: pp 509-26 of Proceedings on the Symposium on Microdosimetry, Ispra, Italy, November 13-15, 1967. Ebert, H. G. (ed.). Brussels, Euratom, 1968.; Other Information: See EUR--3747; CONF-671109. Orig. Receipt Date: 31-DEC-68, 1968: p. Medium: X.
39. Krag, M.H., et al., *Morphometry of the Thoracic and Lumbar Spine Related to Transpedicular Screw Placement for Surgical Spinal Fixation.* Spine, 1988. **13**(1): p. 27-32.
40. Legrand, E., et al., *Trabecular Bone Microarchitecture, Bone Mineral Density, and Vertebral Fractures in Male Osteoporosis.* Journal of Bone and Mineral Research, 2000. **15**(1): p. 13-19.
41. Libouban, H., et al., *Comparison of Histomorphometric Descriptors of Bone Architecture with Dual-Energy X-ray Absorptiometry for Assessing Bone Loss in the Orchidectomized Rat.* Osteoporosis International, 2002. **13**(5): p. 422-428.
42. Rajon, D., et al., *Voxel effects within digital images of trabecular bone and their consequences on chord-length distribution measurements* Physics in Medicine and Biology, 2002. **47**(10).
43. Spiers, F.W. and A.H. Beddoe, *'Radial' scanning of trabecular bone: consideration of the probability distributions of path lengths through cavities and trabeculae (dosimetry).* Physics in Medicine and Biology, 1977. **22**(4): p. 670.

44. Singh, H., et al., *Image based computations of lineal path probability distributions for microstructure representation.* Materials Science and Engineering: A, 2008. **474**(1-2): p. 104-111.
45. Manwart, C., S. Torquato, and R. Hilfer, *Stochastic reconstruction of sandstones.* Physical Review E, 2000. **62**(1): p. 893.
46. Boyard, N., et al., *Study of the porous network developed during curing of thermoset blends containing low molar weight saturated polyester.* Polymer, 2005. **46**(3): p. 661-669.
47. Roberts, A.P., *Statistical reconstruction of three-dimensional porous media from two-dimensional images.* Physical Review E, 1997. **56**(3): p. 3203.
48. Talukdar, M.S., et al., *Stochastic Reconstruction of Chalk from 2D Images.* Transport in Porous Media, 2002. **48**(1): p. 101-123.
49. Bresenham, J., *Algorithm for Computer Control of a Digital Plotter.* IBM Systems Journal, 1965. **4**(1): p. 25-30.
50. Parker, J.A., R.V. Kenyon, and D.E. Troxel, *Comparison of interpolating methods for image resampling.* IEEE Transactions on medical imaging, 1983. **2**(1): p. 31-39.
51. Jokisch, D., et al., *Chord distributions across 3D digital images of a human thoracic vertebra.* Medical physics, 2001. **28**(7): p. 1493-1504.
52. Kellerer, A.M., *Considerations on the random traversal of convex bodies and solutions for general cylinders.* Radiation Research, 1971. **47**(2): p. 359-376.
53. Coleman, R., *Random paths through convex bodies.* Journal of Applied Probability, 1969: p. 430-441.
54. Kellerer, A.M., *Chord-length distributions and related quantities for spheroids.* Radiation research, 1984. **98**(3): p. 425-437.